Supporting Information

Revealing Superoxide-Induced Degradation in Lead-free Tin Perovskite Solar Cells

Zhihao Zhang,[1] Xuesong Tian,[2] Can Wang,[3] Jialun Jin,[1] Yiting Jiang,[1] Qin Zhou,[3] Jingwei Zhu,[1] Jianbin Xu,[3] Rui He,[1] Yuanfang Huang,[1] Shengqiang Ren,[1] Cong Chen,[1] Peng Gao,[3] Run Long,[2*] Dewei Zhao [1*]*

[1] College of Materials Science and Engineering & Engineering Research Center of Alternative Energy Materials & Devices, Ministry of Education, Sichuan University, Chengdu 610065, China
E-mail: dewei.zhao@scu.edu.cn and dewei_zhao@hotmail.com

[2] College of Chemistry, Key Laboratory of Theoretical and Computational Photochemistry of Ministry of Education, Beijing Normal University, Beijing 100875, China
Email: runlong@bnu.edu.cn

[3] CAS Key Laboratory of Design and Assembly of Functional Nanostructures, and Fujian Provincial Key Laboratory of Nanomaterials Fujian Institute of Research on the Structure of Matter Chinese Academy of Sciences Fuzhou, Fujian 350002, China
E-mail: peng.gao@fjirsm.ac.cn

Materials and Methods

Materials

All chemicals were purchased from Sigma Aldrich unless otherwise specified and used without further purification, including dimethyl sulfoxide (DMSO, 99.5%); N, N-dimethylformamide (DMF, 99.99%); chlorobenzene (CB, 99.99%); tin (II) iodide (SnI_2, 99.99%); tin (II) fluorine (SnF_2, 99%); germanium (II) iodide (GeI_2, >99.8%); formamidinium iodide (FAI, >98%); PEDOT: PSS (Clevious PVP AI 4083), BCP (99.9%), and C_{60} were purchased from Xi'an Polymer Light Technology. 1,3-Diphenylisobenzofuran is purchased from Alfa Aesar.

Film and Device Fabrication

The glass substrates coated with indium tin oxide (ITO) were cleaned with detergent, deionized water, and ethanol by ultrasonication for 20 min, respectively. Next, the dried ITO substrates were treated with ultraviolet ozone for 15 min. PEDOT: PSS was then spin-coated onto the ITO at 500 rpm for 10 s followed by 5000 rpm for 30 s and annealed at 170 ^{o}C for 15 min. Then the substrates were transferred into a glove box with a nitrogen atmosphere. The reference perovskite precursor solution was prepared by dissolving FAI, SnI_2, and SnF_2, at a molar ratio of 1.0:1.0:0.1 in the mixed solvent of DMF and DMSO at a volume ratio of 4:1. The modified perovskite precursor solution was prepared by dissolving FAI, SnI_2, $EDAI_2$, and SnF_2, at a molar ratio of 0.99:1.0:0.01:0.1 in the same solvents. The perovskite precursor was filtered with 0.22 μm polytetrafluoroethylene before the spin-coating step. Next, 60 μL precursor was spin-coated onto the substrate at 5000 rpm for 50 s with 500 μL CB dripped onto the perovskite film at 15 s. Then the as-prepared films were annealed at 70 ^{o}C for 30 min. Afterward, C_{60} (25 nm), BCP (6 nm), and Ag (100 nm) were sequentially deposited via thermal evaporation. The resultant active area of 0.0985 cm^2.

Measurement of superoxide yield

The fluorescent molecules DPBF was dissolved in dry toluene, which cannot dissolve perovskite compositions (10 mg/10 mL); Then, the reference or passivated perovskite

films should be Immersed into the above-mixed solution, and avoiding their contact with O_2 and light as much as possible; Next, building a photodegradation condition consisting of continuous illumination by a tungsten halogen lamp and dry O_2 flow bubbled through the organic solvent at a constant flow rate; After regular time intervals, a part of the mixed solutions after light/O_2 treatment is taken out as samples in a sealed container to avoid the contact with O_2 and light; Finally, transferring the above samples in cuvettes for recording the PL spectra using an excitation wavelength of 360 nm, where the corresponding fluorescence intensities at every time interval present the yield of superoxide.

Film and Device Characterizations

The UV-vis absorption spectra for perovskite films were measured by a spectrophotometer (Agilent Cary 5000). The XRD patterns were measured using a Shimazu XRD-6100 diffractometer with Cu-Kα radiation under operation conditions of 40 kV and 30 mA excitation. SEM measurements were performed using a SUPRA 55, Zeiss, Germany, operated at an acceleration voltage of 5 kV. XPS and UPS were carried out using a Thermo Scientific K-Alpha$^+$ (ThermoFisher). Fourier transform infrared (FTIR) spectrum analysis was performed using an FTIR spectrometer (Thermo Scientific Nicolet iS50) with an ATR accessory. The *J-V* curves were measured using Keysight B2901A source meter under AM1.5G (100 mW cm^{-2}) illumination in a N_2-filled glove box with a scan rate of 50 mV s^{-1}. The light intensity was calibrated by the certified standard silicon solar cell (SRC-00205, Enli Tech) with a solar simulator (SS-F5-3A, Enli Tech). External quantum efficiency (EQE) was obtained on a computer-controlled quantum efficiency instrument (QE-R, Enlitech). The solar cells were measured using a black shadow mask with an aperture area of 0.0576 cm^2.

The electrochemical impedance spectroscopy (EIS), Mott-Schottky measurements, thermal admittance spectrum (TAS), and drive-level capacitance profiling (DLCP) were carried out by an electrochemical workstation (Zennium Zahner, Germany). In the DLCP measurement, the DC bias was set from 0 to 0.8 V, and a different AC bias (marked as dV, from 20 to 120 mV) was applied, with the AC frequency held as 10

kHz. The relationship between the capacitance and applied AC bias can be described by $\frac{C}{dV} = C_0 + C_1 dV + C_2(dV)^2 + C_3(dV)^3 \ldots$ After recording the data, C_0 and C_1 can be obtained by fitting. The trap density (N_T) and the profiling distance (x) can be calculated by $N_T = -\frac{{C_0}^3}{2q\varepsilon\varepsilon_0 A^2 C_1}$ and $X = \varepsilon\varepsilon_0 A/C_0$, respectively. Here, q, ε, ε_0, and A represent the elementary charge, the relative permittivity of perovskite materials, vacuum permittivity, and active area, respectively.

The aging condition of light/O_2 environment for $FASnI_3$ devices was achieved in a desiccator (QHD260, ZISOdry) at room temperature (25 °C) with constant LED illumination (100 mW cm^{-2}).

DFT Calculations

DFT calculations were performed with Vienna ab initio Simulation Package (VASP).[1] The Perdew-Burke-Ernzerhof (PBE) functional projected-augmented wave method was used to treat the interactions of electron exchange-correlation and ionic cores-valence electrons, respectively.[2,3] A cutoff energy was set to 500 eV along with a 2 × 3 × 1 Monkhorst-Pack mesh to sample the Brillouin zone.[4] The energy and force convergence criteria were set to 10^{-4} eV and 0.05 eV/Å for geometry optimization, respectively. To eliminate the size influence on phase map and defect formation energy in two perovskites, a 96-atom supercell of 2 × 2 × 2 cubic phase ($Pm\bar{3}m$) $FAPbI_3$ and 2 × 1 × 2 orthorhombic phase (*Amm2*) $FASnI_3$ was used.[5] The calculated bandgaps of $FAPbI_3$ and $FASnI_3$ of 1.35 and 1.50 eV are in good agreement with the experimental value of 1.47 eV[6] and 1.41 eV, respectively.[5] The mutual agreement arises from the cancellation of errors composed of an electron self-interaction in PBE functional and lack of spin-orbit coupling, as demonstrated in previous works.[7]

The phase diagram offers a virtual picture of how $FAPbI_3$ and $FASnI_3$ can be formed and stabilized as a function of the element chemical potentials. Under thermodynamic equilibrium growth conditions. the existence of $FAPbI_3$ should satisfy the following

criteria:

First, the formation of the elemental phase should be avoided that $\Delta\mu_i$ (i = Pb, I, and FA) requires to be smaller than 0.

$$\Delta\mu_{Pb} = \mu_{Pb} - {\mu_{Pb}}^0 < 0 \quad (1)$$

$$\Delta\mu_I = \mu_I - {\mu_I}^0 < 0 \quad (2)$$

$$\Delta\mu_{FA} = \mu_{FA} - {\mu_{FA}}^0 < 0 \quad (3)$$

Here, ${\mu_i}^0$ is the atomic energy of the most stable elemental phase. ${\mu_{Pb}}^0$ and ${\mu_I}^0$ are calculated using solid lead in the cubic phase and solid iodine in the orthorhombic phase, respectively. ${\mu_{FA}}^0$ is obtained by putting a single FA in a cubic box and optimizing it.

Second, the chemical potentials of FA, I, and Pb must satisfy the following constraints to exclude the possible secondary phase PbI_2 (trigonal phase) and $CH(NH_2)_2I$ (FAI, rock-salt phase):

$$\Delta\mu_{FA} + \Delta\mu_I < \Delta H_f(FAI) = -2.31\ eV \quad (4)$$

$$\Delta\mu_{Pb} + 2\Delta\mu_I < \Delta H_f(PbI_2) = -1.96\ eV \quad (5)$$

At the same time, the chemical potentials follow the relationship to maintain a stable $FAPbI_3$ compound:

$$\Delta\mu_{FA} + \Delta\mu_{Pb} + 3\Delta\mu_I = \Delta H_f(FAPbI_3) = -4.65\ eV \quad (6)$$

Here, $\Delta H_f(FAPbI_3)$ is the formation energy of $FAPbI_3$ with respect to the elemental phases.

Similar to $FAPbI_3$, the formation of stable $FASnI_3$ has the same constraints described by equations (1)-(4) of which the subscript Pb in equation (1) is replaced with Sn subject to metal Sn with tetragonal phase. Equations (7-9) guarantee the exclusion of the secondary phase of SnI_2 (monoclinic phase), SnI_4 (cubic phase), and FA_2SnI_6 (cubic phase):

$$\Delta\mu_{Sn} + 2\Delta\mu_I < \Delta H_f(SnI_2) = -1.51\ eV \quad (7)$$

$$\Delta\mu_{Sn} + 4\Delta\mu_I < \Delta H_f(SnI_4) = -1.61\ eV \quad (8)$$

$$2\Delta\mu_{FA} + \Delta\mu_{Sn} + 6\Delta\mu_I < \Delta H_f(FA_2SnI_6) = -7.56\ eV \quad (9)$$

Considering the thermodynamic equilibrium conditions, the formation of $FASnI_3$ should satisfy:

$$\Delta\mu_{FA} + \Delta\mu_{Sn} + 3\Delta\mu_I = \Delta H_f(FASnI_3) = -4.36\ eV \quad (10)$$

The above computational procedure and constraints lead to the phase diagrams of $FAPbI_3$ and $FASnI_3$ in Figure 3a-3b, respectively, of which the narrow red region defines the growth conditions for synthesizing stable and stoichiometric $FAPbI_3$ and $FASnI_3$ under thermodynamic equilibrium conditions. Synthesis of both stable perovskites, particularly for the $FAPbSn_3$ due to the presence of additionally competing secondary SnI_4 and FA_2SnI_6 compounds, is required to carefully regulate the growth conditions.

Following the derived phase diagram, the formation energy of an iodine vacancy (V_I) was calculated using the unique values of element chemical potential in the red ranges, according to the equation (11):

$$E_f(V_I) = E(V_I) - E(host) + \mu_i \quad (11)$$

Here, $E(V_I)$ and $E(host)$ are the total energies of $FAPbI_3$/$FASnI_3$ with and without a V_I defect. Chemical potentials μ_i (i=Pb, Sn) relies on real growth conditions and can be calculated by $\mu_i = \Delta\mu_i + \mu_i^0$ in terms of that $\Delta\mu_i$ can read directly from the phase map, Figure 3A-3B. Apparently, defect formation energy $E_f(V_I)$ is a function of μ_i. The formation energy of an O_2 incorporating into the V_I-contained $FAPbI_3$ and $FASnI_3$ is computed according to equation (12):

$$E_f(O_2) = E(V_I + O_2) - E(O_2) - E(V_I) \quad (12)$$

Where $E(V_I + O_2)$ is the total energy of the V_I-contained perovskite with an O_2 molecule in the V_I site, and $E(O_2)$ is the energy of an isolated O_2 molecule at its triplet state.

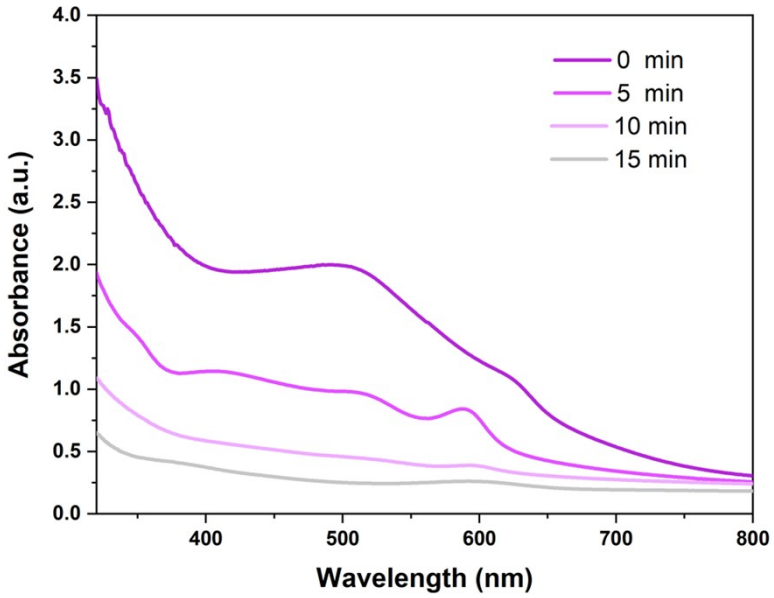

Fig. S1 Absorption spectra of $FASnI_3$ film with light/O_2 exposure with time.

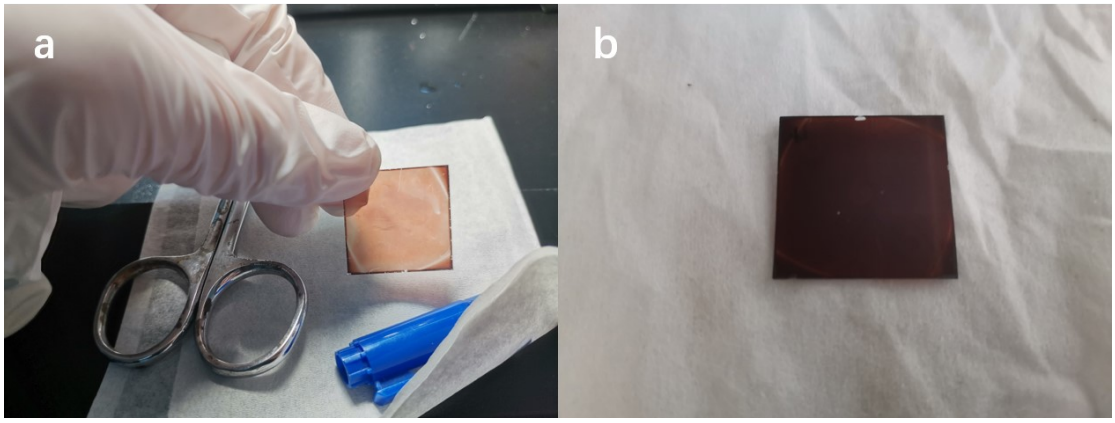

Fig. S2 Photos of (a) $FASnI_3$ film and (b) $FAPbI_3$ film after 5-min light/O_2 exposure.

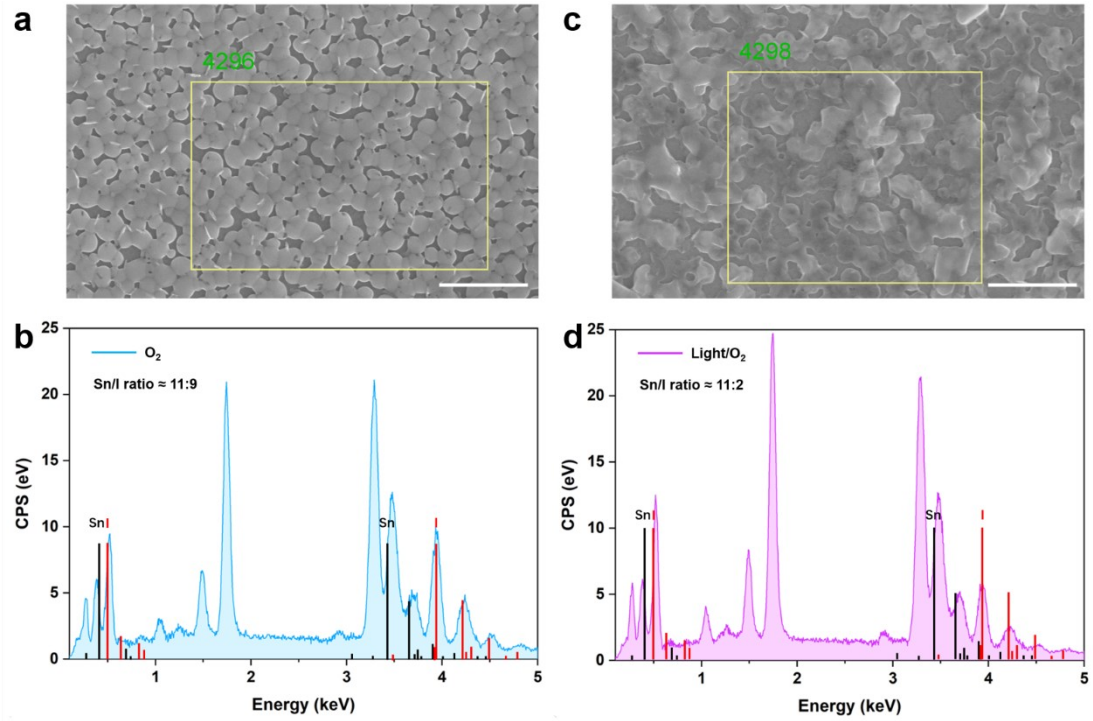

Fig. S3 Selected regions in SEM images and corresponding EDS spectroscopy of $FASnI_3$ films with only (a-b) O_2 exposure and (c-d) light/O_2 exposure. The scale bar is 4 μm.

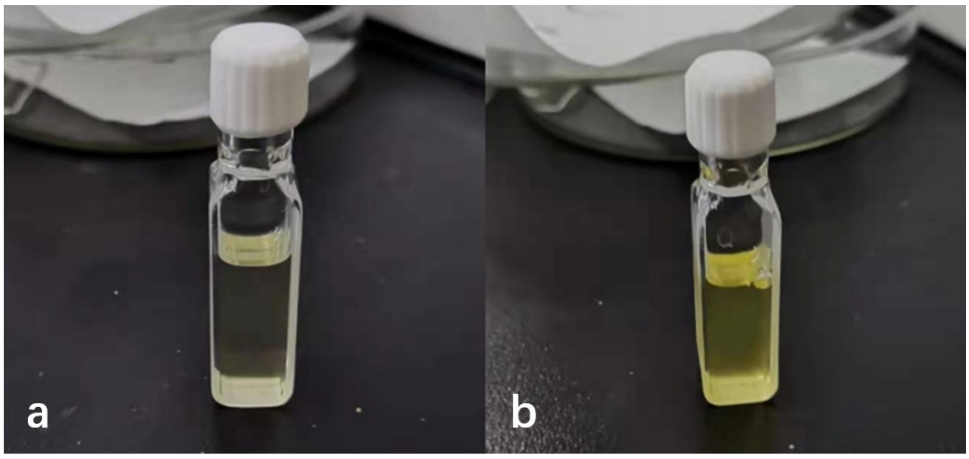

Fig. S4 Color change of the toluene solution. The color of the solution gradually turns from (a) faint yellow to (b) deep yellow with the increased amounts of degraded samples under O_2/light exposure.

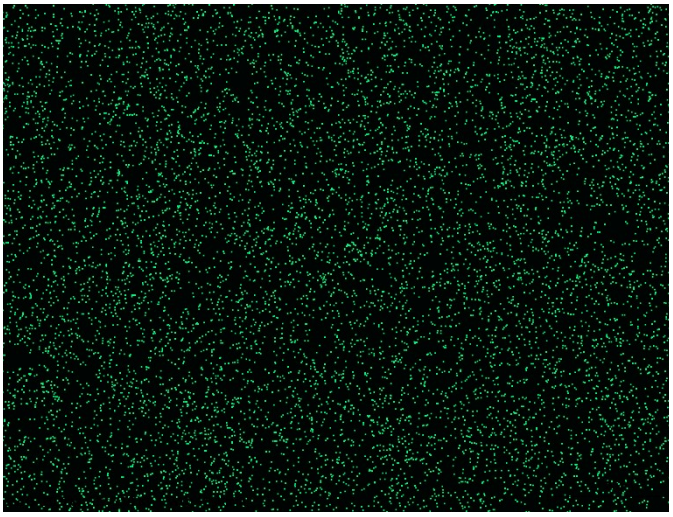

Fig. S5 EDS elemental mapping of O for the $FASnI_3$ film after light/O_2 exposure.

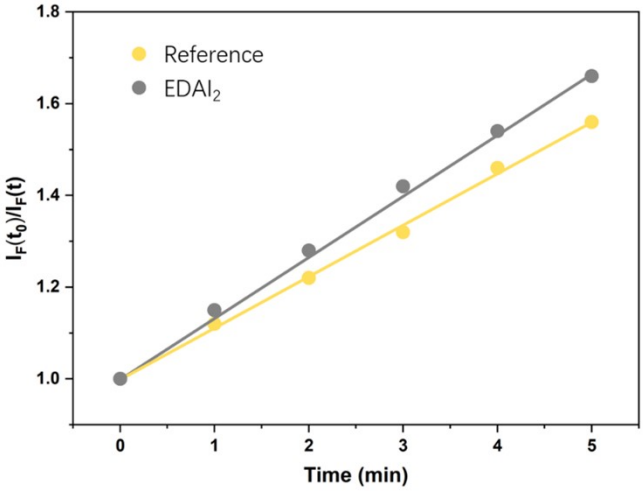

Fig. S6 Superoxide generation yields for $FASnI_3$ modified with additives and without $EDAI_2$.

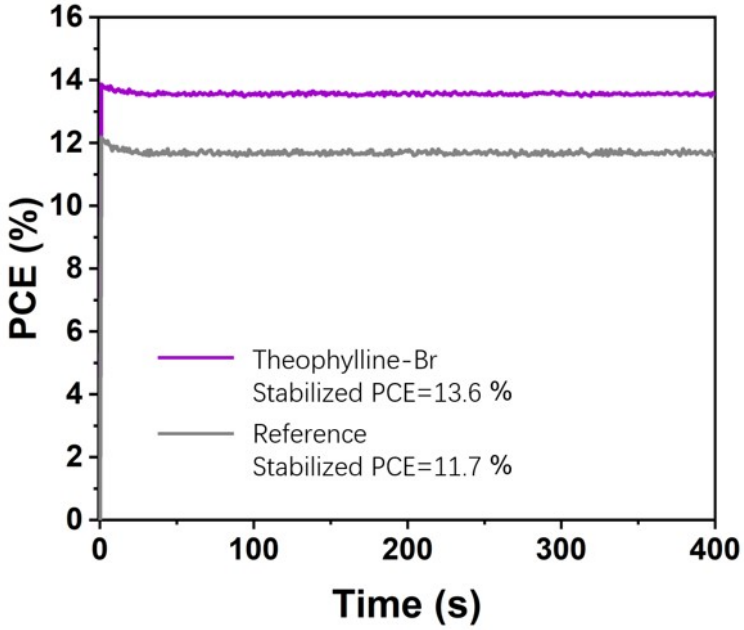

Fig. S7 MPP tracking of the best-performing reference and theophylline-Br modified devices under AM 1.5 G 100 mW cm^{-2} illumination.

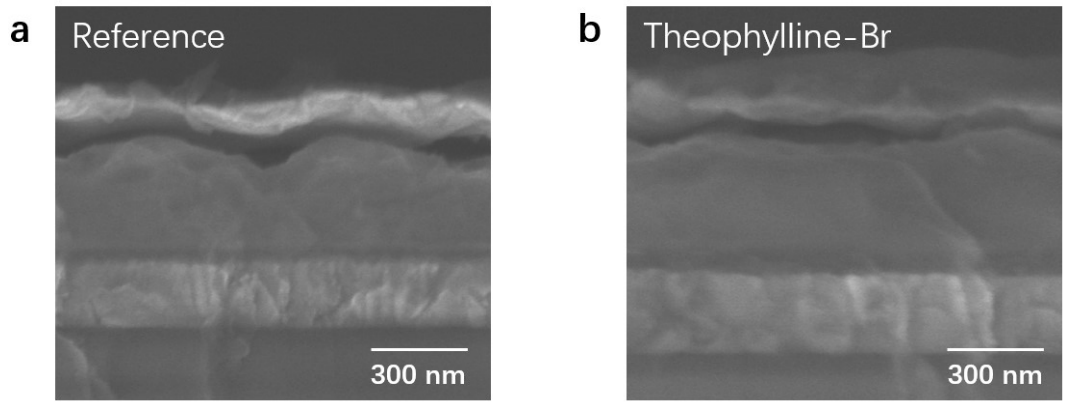

Fig. S8 Cross-sectional images of (a) reference and (b) theophylline-Br modified PSCs.

Table S1 Percentages of Sn^{2+} and Sn^{4+} calculated from XPS data.

Sample	Sn^{4+}	Sn^{2+}
Control	6.1%	93.9%
O_2	53.2%	46.8%
Light/O_2	70.8%	29.2%

Table S2 The $I_F(t0)/I_F(t)$ values of the modified samples with different concentrations after 5-min light/O_2 exposure. The optimal concentration in bold of theophylline-Br to reduce superoxide formation is used for further device fabrication.

Additive	Concentration (mg/mL)			
	1	2	4	8
Choline-Cl	1.63	**1.62**	1.74	1.80
Choline-Br	1.36	**1.29**	1.44	1.75
Theophylline-Cl	**1.42**	1.55	1.63	1.62
Theophylline-Br	**1.08**	1.22	1.42	1.64

Table S3 Summary on statistical photovoltaic parameters of the theophylline-Br modified and reference PSCs (10 devices for each type), as well as their best-performing devices under reverse and forward scan. The hysteresis index (HI) is calculated using the values of average PCE by equation $HI = (PCE_{RS} - PCE_{FS})/PCE_{RS}$.

Sample		J_{SC} (mA cm^{-2})	V_{OC} (V)	FF	PCE (%)	HI
Reference	reverse	23.5±0.31	0.70±0.02	0.70±0.03	11.5±0.5	0.026
	champion	**23.8**	**0.72**	**0.71**	**12.1**	
	forward	23.5±0.22	0.68±0.02	0.70±0.02	11.2±0.4	
	champion	**23.8**	**0.71**	**0.70**	**11.8**	
Theophylline-Br	reverse	24.3±0.11	0.74±0.01	0.75±0.01	13.6±0.2	0.007
	champion	**24.2**	**0.75**	**0.76**	**13.8**	
	forward	24.1±0.10	0.73±0.01	0.76±0.00	13.5±0.17	
	champion	**24.1**	**0.75**	**0.76**	**13.7**	

Table S4 Fitting parameters for TRPL decays from theophylline-Br modified and reference $FASnI_3$ films. The TRPL plot exhibited in Fig. 5h was fitted with a bi-exponential decay function defined as: $I = A_1 exp(-t/\tau_1) + A_2 exp(-t/\tau_2)$.

Sample	τ_1 (ns)	A_1	τ_2 (ns)	A_2	τ_{ave} (ns)
Reference	3.9	0.14	1.9	4.0	2.0
Theophylline-Br	5.0	1.43	10.8	0.24	6.5

References

1 G. Kresse and J. Furthmüller, *Phys. Rev. B - Condens. Matter Mater. Phys.*, 1996, **54**, 11169–11186.

2 J. P. Perdew, K. Burke and M. Ernzerhof, *Phys. Rev. Lett.*, 1996, **77**, 3865–3868.

3 P. E. Blöchl, *Phys. Rev. B*, 1994, **50**, 17953–17979.

4 D. J. Chadi, *Phys. Rev. B*, 1977, **16**, 1746–1747.

5 C. C. Stoumpos, C. D. Malliakas and M. G. Kanatzidis, *Inorg. Chem.*, 2013, **52**, 9019–9038.

6 T. M. Koh, K. Fu, Y. Fang, S. Chen, T. C. Sum, N. Mathews, S. G. Mhaisalkar, P. P. Boix and T. Baikie, *J. Phys. Chem. C*, 2014, **118**, 16458–16462.

7 J. Even, L. Pedesseau, J. M. Jancu and C. Katan, *J. Phys. Chem. Lett.*, 2013, **4**, 2999–3005.